Photosynthetic Solar Cell Using Nanostructured Proton Exchange Membrane for Microbial Biofilm Prevention

Dong Hyun Lee,[†] Hwa Jin Oh,[‡] Seoung Jae Bai,[§] and Young Seok Song[†,*]

[†]Department of Fiber System Engineering, Dankook University, 126 Jukjeon-dong, Suji-gu, Yongin-si, Gyeonggi-do 448-701, Korea, [‡]Samsung Display, Samsung st 181, Tangjeong-Myeon, Asan-City, Chungcheongnam-do Korea, and [§]Department of Mechanical Engineering, Dankook University, 126 Jukjeon-dong, Suji-gu, Yongin-si, Gyeonggi-do 448-701, Korea

ABSTRACT Unwanted biofilm formation has a detrimental effect on bioelectrical energy harvesting in microbial cells. This issue still needs to be solved for higher power and longer durability and could be resolved with the help of nanoengineering in designing and manufacturing. Here, we demonstrate a photosynthetic solar cell (PSC) that contains a nanostructure to prevent the formation of biofilm by micro-organisms. Nanostructures were fabricated using nanoimprint lithography, where a film heater array system was introduced to precisely control the local wall temperature. To understand the heat and mass transfer phenomena behind the manufacturing and energy harvesting processes of PSC, we carried out a numerical simulation and experimental measurements. It revealed that the nanostructures developed on the proton exchange membrane enable PSC to produce enhanced output power due to the retarded microbial attachment on the Nafion membrane. We anticipate that this strategy can provide a pathway where PSC can ensure more renewable, sustainable, and efficient energy harvesting performance.

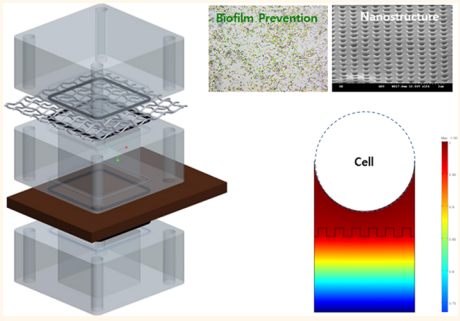

KEYWORDS: biofilm · nanostructure · nanoimprint lithography · energy harvesting

Many techniques have been developed to fabricate nanostructures including top-down methods, such as photolithography,[1] soft lithography,[2] nanoimprint lithography,[3] and scanning probe lithography,[4] and bottom-up methods such as plasma arcing,[5] chemical vapor deposition,[6] molecular beam epitaxy,[7] and molecular self-assembly.[8,9] In most cases, these methods require precise processing condition control and sophisticated tools. Nanoimprint lithography (NIL) is a simple patterning process that can transfer nanostructure into polymer by pressing a mold. Recently, a considerable amount of research has been carried out on NIL since it can serve as a new generation lithography tool to be used in manifold applications such as semiconductors, sensors, grating, filters, polymer lasers, and lenses.[10−12] In terms of mass production, the NIL is strongly competitive compared with conventional e-beam lithography and X-ray lithography as it enables the production of large areal complex patterns at relatively low cost with high resolution.[13]

Biofilms are populations of micro-organisms that are irreversibly attached to a substratum, to an interface, and/or to each other. Also, biofilms imply a survival mechanism in microbial communities colonizing surfaces or interfaces where growth is possible.[14−16] They are typically surrounded by a matrix of extracellular polymeric substances (*i.e.*, polysaccharides and proteins) that they produce[17−20] and can be found in various environments such as underwater, membranes, groundwater, and biomedical applications. Since microbial biofilms can reduce the performance of engineered systems in unexpected ways such as biofouling, infection, failure of medical devices, and biocorrosion, their growth control is critical to achieve reliable long-term efficiency.[21,22]

In general, biofilms show a relatively high resistance to antibiotics and antimicrobial agents compared to planktonic bacteria of

* Address correspondence to ysong@dankook.ac.kr.

Received for review April 12, 2014 and accepted May 19, 2014.

Published online May 19, 2014
10.1021/nn502033f

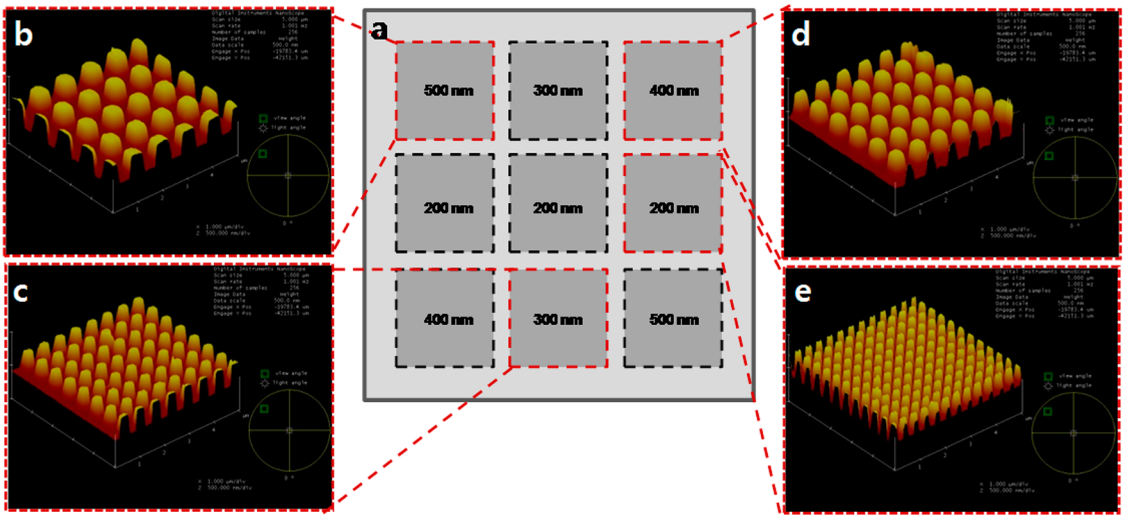

Figure 1. Schematic illustration of the Ni stamp fabricated: (a) layout of the nanopatterns on the stamp and (b−e) AFM images of the nanopatterns.

the same species due to their protective microenvironment, where biocidal activities are decelerated, and the transfer of nutrients and ions from the environment is limited. It has been known that the surface roughness of the substratum plays a key role in determining the interaction between the cells and the surface and forming the resulting biofilms.[23−25] In particular, a nanostructured surface manipulates the biofilm formation, but the relevant mechanism remains poorly understood. For analyzing such biofilms, microscopical, molecular biological, chemical, and physical methods have been employed.[26]

Bioenergy involving solar energy conversion by plants or algae has attracted enormous attention for sustainable renewable energy production including biomass and biofuels. In particular, bioelectricity has been regarded as a promising electrical energy source.[27] Unlike a conventional microbial fuel cell, the photosynthetic solar cell (PSC) or photosynthetic microbial fuel cell employs solar energy by combining photosynthetic micro-organisms with microbial fuel cell systems.[28−33] Even if a conversion efficiency as promising as 3%, which is similar to the value of organic solar cells, is reported, many issues need to be solved in such an energy harvesting system.[34] For example, expensive catalysts and toxic mediators are used for hydrogen oxidation and electron siphoning, respectively.[35,36]

In the current study, we develop a PSC system that provides higher output power and longer durability by introducing a nanostructure to the proton exchange membrane (PEM). For this, we propose a new fabrication system where a film heater array is embedded to precisely control the processing temperature. With the help of nanoimprint lithography, a nanopattern is transferred to a Nafion film, and the biofilm growth on the film is investigated to examine the effect of the nanostructure on biofilm prevention.

RESULTS AND DISCUSSION

Four nanopillar groups with different diameter sizes (*i.e.*, 200, 300, 400, and 500 nm) were designed and arranged on a Ni stamp, as shown in Figure 1. The Ni stamp with dimensions of 12 cm × 12 cm × 0.8 cm, where nine sections with different nanopatterns were constructed, was identified by using atomic force microscopy (AFM). One of the key factors for successfully producing a nanosized polymeric structure is to precisely control the local wall temperature of a mold. The fabricated film heater array system allows us to control the wall temperature in a spatial and temporal manner with high accuracy. The film heater array, which is composed of nine independent modules, is positioned beneath the Ni stamp to transfer heat efficiently. The configuration of the heater array and the stamp is illustrated in Figure 2. Before performing the nanoimprint lithography for the MEA fabrication (Figure 3a), the Pt deposition was carried out as shown in Figure 3b. Figure 3c presents a comparison between a pristine and the nanostructured Nafion film on the carbon cathode. Further details are explained in Supporting Information.

To provide insight into designing the film heater array and to determine the optimal processing conditions for nanoimprint lithography, we carried out a numerical simulation on the heat transfer. Figure 4a,b presents the resulting temperature contours on the stamp. The insets of the graphs present the location of the heater when it is turned on. It is verified that the heat modules work independently and that a sufficiently high-temperature distinction between the partitions is developed. The proton diffusion through Nafion films was modeled numerically (Figure 4c,d).

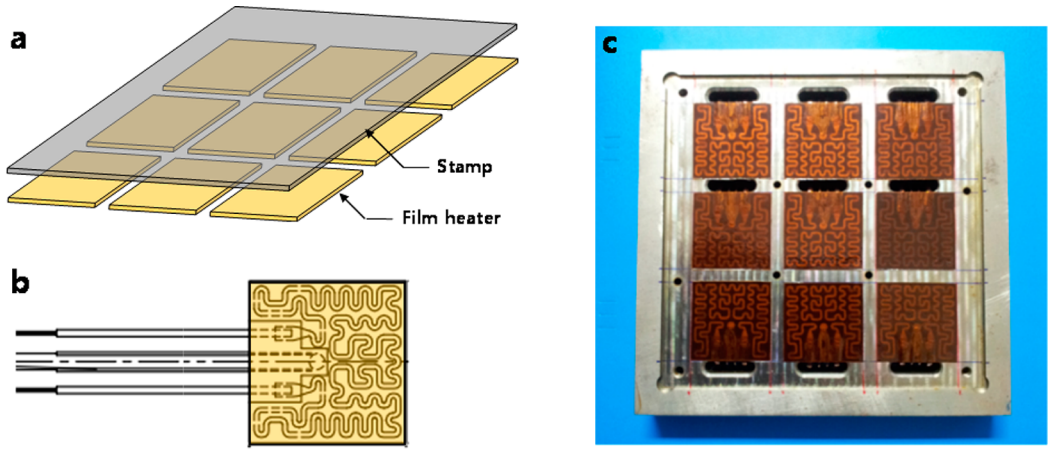

Figure 2. Film heater array system: (a) schematic diagram of configuration of the Ni stamp and the film heater array, (b) pattern of nichrome wire, and (c) assembly of the film heater array.

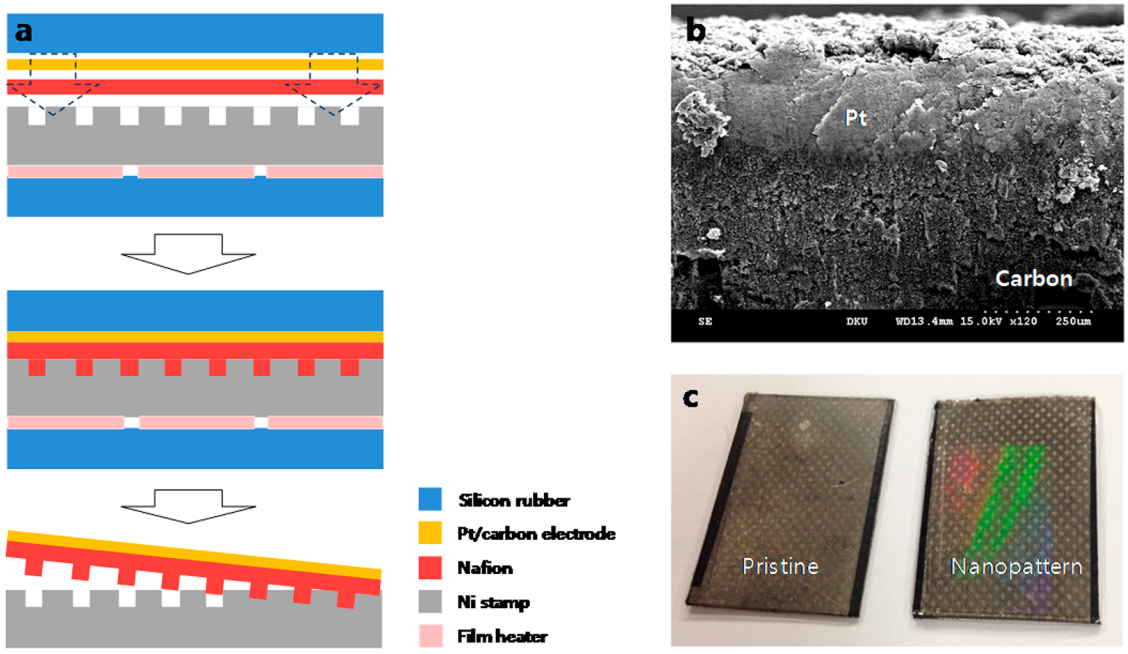

Figure 3. (a) Schematic illustration of the MEA fabrication with use of nanoimprint lithography, (b) SEM image of the Pt-deposited carbon electrode, and (c) comparison between pristine and nanopatterned Nafion films.

The nanostructures increase the effective diffusivity of protons and the interfacial area between the Nafion and the cell medium, thereby leading to multidirectional diffusion rather than unidirectional diffusion at the interface. However, the effect is found to be not as remarkable as expected since the mass transfer is governed mainly by the averaged bulk properties and geometric characteristics.

After the nanoimprinting process was applied, the tensile strength, Young's modulus, and elongation at break were all increased compared to the untreated sample (Figure 5a). This is attributed to the enhancement in the crystallinity of Nafion induced by the heat treatment. In this sense, the linear swelling ratio shows the reverse order (Figure 5b). That is, the pristine Nafion has the highest linear swelling ratio, while the Nafion film treated at 150 °C gives the lowest linear swelling ratio. The corresponding crystalline characteristics are explained in Figure 5c,d. As the treatment temperature increases, the resulting glass transition temperature (*i.e.*, order−disorder transition of ionic clusters) and enthalpy of crystallization (*i.e.*, melting of microcrystalline regions) are found to increase.[37] The enthalpy of the evaporation of water indirectly indicates the content of water in the Nafion samples.

As aforementioned, the wall temperature is controlled in order to determine an optimal processing condition for the high pattern quality in the nanoimprint lithography. Figure 6 presents SEM images of the

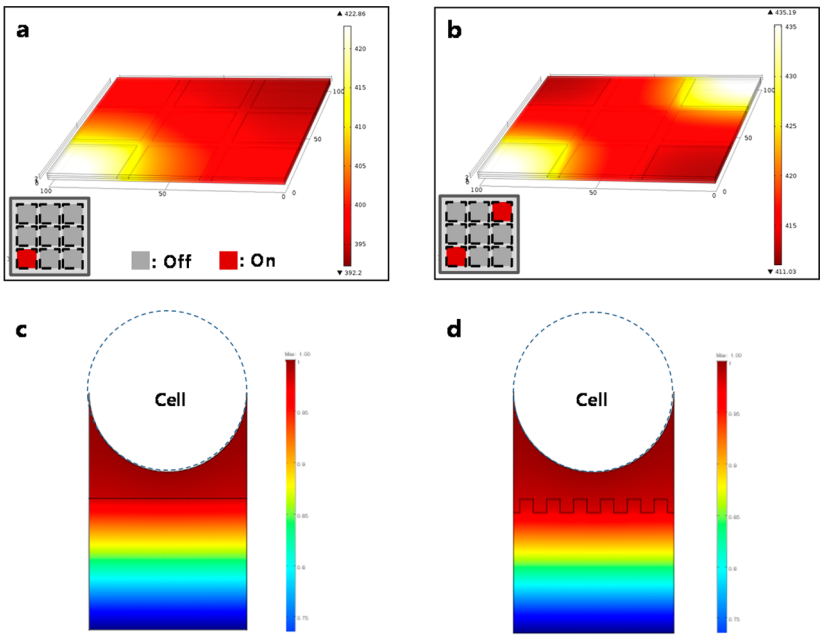

Figure 4. Results of numerical simulation: (a,b) temperature contours on the Ni stamp controlled by the proposed film heater array system and (c,d) diffusion behaviors of protons through the Nafion membrane.

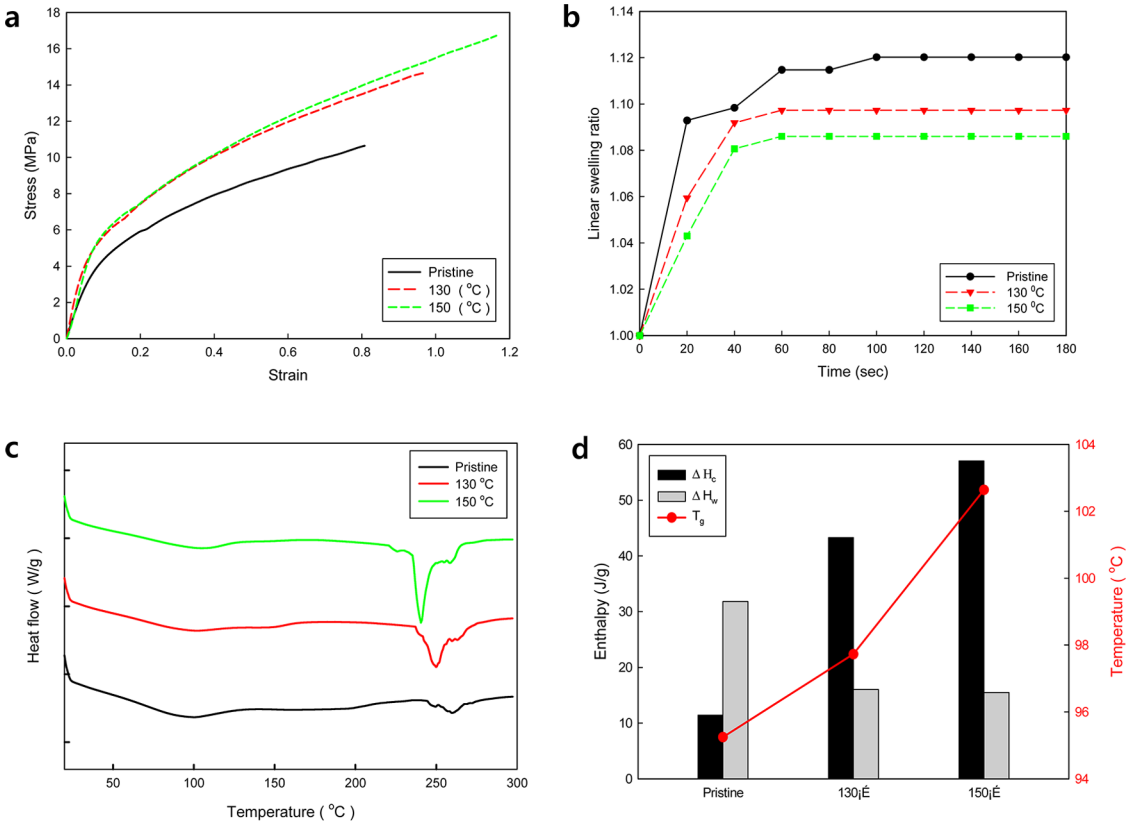

Figure 5. (a) Stress−strain curve for Nafion membranes, (b) linear swelling ratio as a function of time, (c) differential thermograms for the samples treated with different temperatures, and (d) variation in the enthalpy and glass transition temperature (ΔH_c, the enthalpy of crystallization; ΔH_w, the enthalpy of evaporation of water).

specimens with different nanopatterns. The samples nanoimprinted at 130 °C have poor pattern resolution, while the other samples show quite good replication quality, even in the case of the smaller pattern size. It is worth noting that, for nanoimprint lithography, the increase of the surface area generally results in

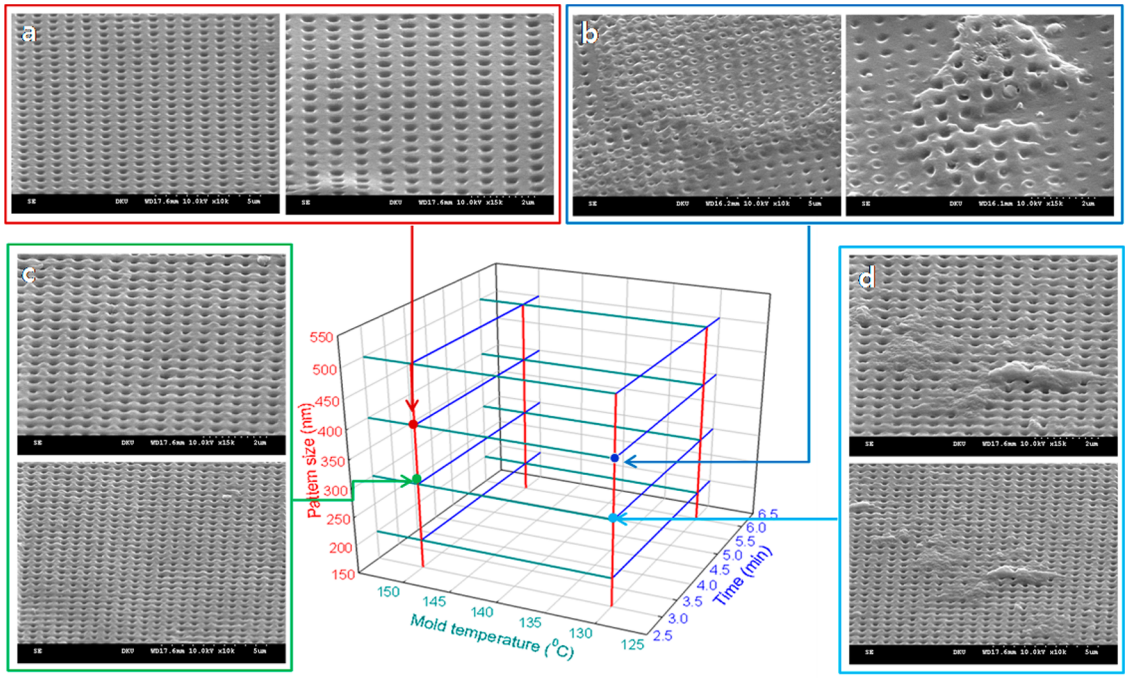

Figure 6. SEM images and processing conditions of the Nafion specimens prepared by using nanoimprint lithography. At the fixed time, the mold temperature and pattern size were considered as processing variables.

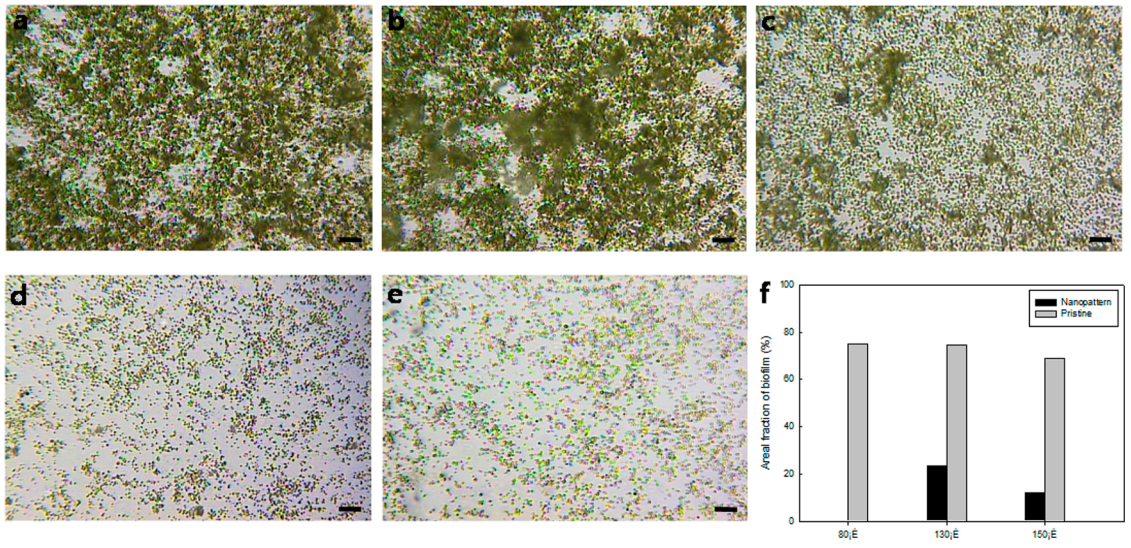

Figure 7. Microscopic images of algal biofilm: (a−c) bare Nafion membranes treated at 80, 130, and 150 °C, respectively, and (d,e) nanopatterned Nafion membranes prepared at 130 and 150 °C, respectively. (f) Variation of the areal fraction of biofilm with respect to the mold temperature. The scale bars indicate 50 μm.

deformation and breakage of the molded pattern due to the large interfacial energy between the molded polymer and the mold wall. Additional results are explained in Supporting Information.

Figure 7 shows the results of analyzing the biofilm formation on the Nafion membrane. Compared with the images for the bare Nafion films (Figure 7a−c), the nanopatterned Nafion films show a significantly low degree of biofilm formation (Figure 7d,e). This demonstrates that the nanostructure on the Nafion film retards biofilm formation. These findings indicate that while biofilm formation is a complex and multifactorial phenomenon, surface topography (*i.e.*, nanopatterning) yields an apparently different micro-organism growth behavior. To quantitatively evaluate the antibiofilm activities, the microscopy images were analyzed using an image processing program, ImageJ. Figure 7f presents the areal fraction of the biofilms with respect to the processing conditions. The Nafion film prepared at 150 °C shows the lowest value, which means that the well-patterned nanostructures enable the prevention of biofilm formation.

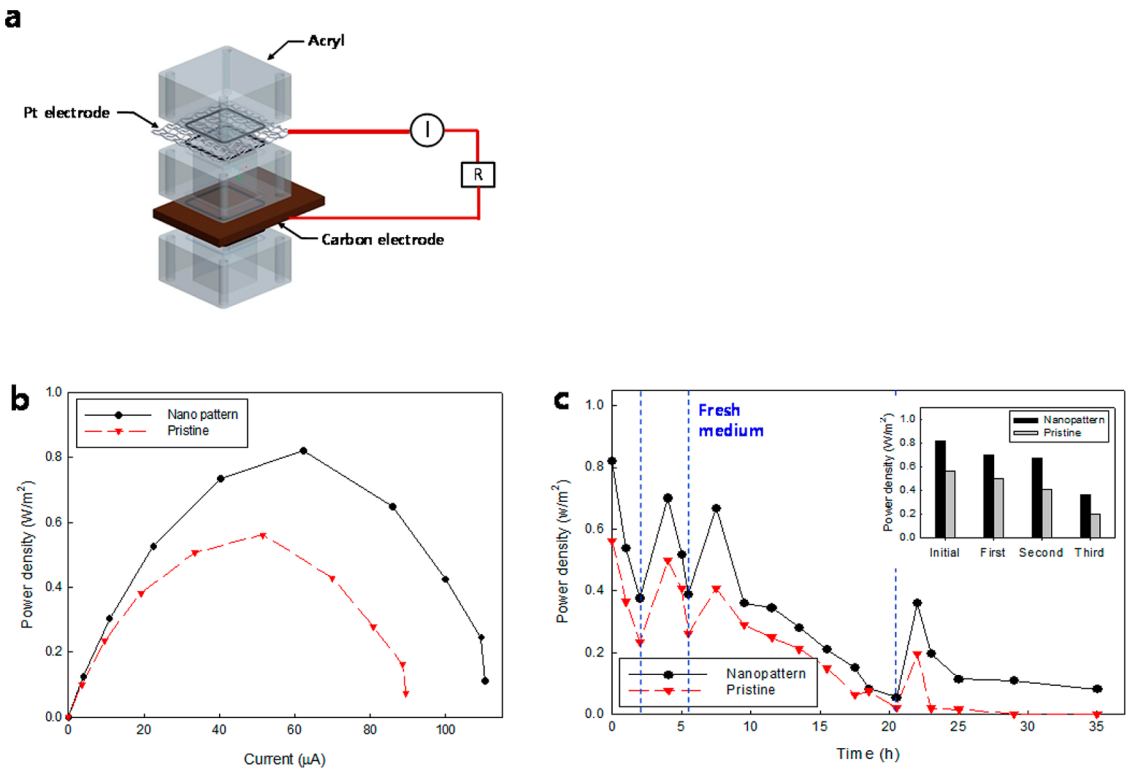

Figure 8. (a) Schematic view of the photosynthetic solar cell used in this study, (b) variation of power density with respect to current, and (c) power density as a function of time. The inset shows the change of the power densities at the peaks. The blue dashed lines represent the refreshment of cell medium.

Unlike microbial fuel cells, a photosynthetic solar cell needs a transparent environment where light penetrates into the cell chamber. The experimental setup adopted in this study is demonstrated in Figure 8a. For the anode and cathode, a Pt mesh and a carbon paper were employed, respectively. The Nafion membrane with the nanopattern fabricated using nanoimprint lithography was used as a PEM. Once an on-light stimulus is applied to the cells, the measured current gradually increases over time. During the photosynthesis triggered by light, high-energy electrons are generated and transported through the photosystems in the thylakoid membranes. During the transportation, redox mediator molecules in the chamber extract such electrons from the photosystems and bring them to the anode. The electrons move through an external load and are eventually reduced with oxygen and protons at the cathode. When the current reached the steady state, we increased the resistive loads (see Figure S7). The resulting output power density is shown in Figure 8b. The PSC with nanopatterns is found to offer higher power than that with a bare Nafion membrane. This indicates that the nanostructures on the Nafion membrane not only lead to the prevention of the biofilm formation, which is in accordance with the results presented in Figure 7, but also are more advantageous in transferring the proton through the membrane.

As reported in the literature, the redox mediator is harmful to algae. As a result, the measured power density diminished over time (Figure 8c). In order to identify the long-term performance of the PSC, we refreshed the cell medium regularly. The inset presents the change of the peak power densities immediately after refreshing the medium. While the overall power density decreases over time, it is evident that the PSC containing the nanopatterned Nafion membrane provides greater energy harvesting performance than the control sample. In this way, the innovative manufacturing system introduced in the present study was successfully applied to enhance the PSC performance.

CONCLUSION

We developed a photosynthetic solar cell that can improve the energy harvesting efficiency for algae by introducing nanostructures into the PEM membrane. For more robust and reliable fabrication of the nanostructures, a new film heater array system, able to spatially and temporally control the wall temperature, was applied to nanoimprint lithography. Heat and mass transfer phenomena were numerically modeled to understand the underlying physics behind the design and fabrication process. MEA containing the nanoimprinted Nafion film was fabricated using the heater array system. The antibiofilm activity of the nanostructure was analyzed using a microscopical method. The finding shows that the nanopattern of the Nafion membrane inhibits micro-organisms from attaching and growing onto the surface. The PCS with

the nanostructured Nafion membrane provided enhanced output power density compared with the control case, which can be explained by the prevention of biofilm formation for algae. We foresee that the nanostructure-embedded PCS platform is poised to serve as a new strategic pathway toward enhancing energy production and maintaining long-term performance of devices in biofilm-related energy harvesting areas.

METHODS

Stamp Design and Fabrication. Microelectromechanical system techniques were employed to materialize the designed pattern on the mold stamp, which has a complementary pattern to that of the resulting products fabricated using nanoimprint lithography. A detailed explanation on the patterning procedure is presented in Supporting Information. The Ni stamp prepared using the electroforming process was cut to the proper size for installation in a nanoimprinting machine using a wire cutting method.

Fabrication of a Film Heater Array System. It is essential to precisely control the wall temperature in order to replicate nanostructures with a high pattern quality in nanoimprint lithography. However, a conventional heating system using nanoimprint lithography is not suitable for acquiring an accurate local wall temperature. A new film heater array system was thus designed and fabricated in this study. As shown in Figure 2, the system was partitioned into nine sections. Each section consists of a single film heater with dimensions of 3 × 3 × 0.7 cm^3. Its heating and cooling rates were 100 °C/min, and maximum temperature was 200 °C. The temperatures of the nine sections were controlled separately by each controller.

Membrane Electrode Assembly. The Nafion-117 membrane (180 μm thick, EW1100) was purchased from Dupont. The membrane was first treated with 0.5 M H_2O_2 at 80 °C for 1 h and then rinsed with boiling water for 1 h. Thereafter, it was treated with 0.5 M H_2SO_4 at 80 °C and again rinsed with boiling water for 1 h. For the fabrication of the MEA structure, 200 nm Pt was deposited on a carbon electrode (ADE75, MEET) by using an evaporator. Following the typical manufacturing method for an air cathode, the Pt-coated carbon electrode and the Nafion membrane were bonded *via* hot pressing. Simultaneously, the polymer membrane was nanoimprinted using the Ni mold, where the film heater array system controlled the wall temperature (130 or 150 °C). The hot pressing pressure and time were 0.5 MPa and 5 min, respectively.

Measurements. Morphological analyses were carried out using an atomic force microscope (Nanoman, Hitachi) and a field emission electron microscope (JEOL, JSM-5410LV). For the SEM characterization, a Pt layer of 6 nm was coated on the samples using an ion sputter coater (JEOL, JFC-1100E). Tensile tests were conducted at room temperature using a universal testing machine (Universal Testing Machine 3365, Instron) according to the ASTM 3039. The crosshead speed was set to 5 mm/min. In each case, at least five measurements were carried out. The thermal characteristics of specimens were investigated using differential scanning calorimetry (DSC, Mettler Toledo DSC-822E). The samples were scanned between 25 and 300 °C at ±20 °C/min. The linear swelling ratio (LSR) was determined: LSR = L_s/L_o, where L_o and L_s are the lengths of the Nafion membrane before and after immersion in water, respectively. The sample for measuring the LSR was immersed in distilled water at 25 °C, and the degree of swelling of the Nafion membrane was measured with respect to time. *Chlorella vulgaris* (ATCC 9765) was selected as an algal cell in this study and grown in a BG-11 medium with shaking at 37 °C. The nanopatterned Nafion membrane was immersed in the cell suspension, and the resulting microbial biofilm formation on the membrane was observed with a microscope (Leitz, ORTHOPLANE). To siphon electrons from algae, 2,5-dimethyl-1,4-benzoquinone was used as a mediator. Amperometric experiments were conducted using a potentiostat, VeraStat 3 (Princeton Applied Research, USA) in a two-electrode system. The maximum power was measured at different resistances.

Simulation. To ensure a more systematic design for the nanostructure fabrication platform and to provide a more in-depth understanding on the MEA structure, we carried out a numerical simulation on the relevant heat transfer and mass diffusion. Let us start with the following assumptions: (i) incompressible flow, (ii) Newtonian flow, and (iii) three-dimensional conduction and convection. The corresponding governing equations are as follows:

$$\rho \frac{D\mathbf{u}}{Dt} = \mu \nabla^2 \mathbf{u} - \nabla P + \rho \mathbf{g} \quad (1)$$

$$\nabla \cdot \mathbf{u} = 0 \quad (2)$$

$$\rho C_p \frac{DT}{Dt} = k \nabla^2 T \quad (3)$$

$$\frac{Dc}{Dt} = D \nabla^2 c + R \quad (4)$$

where μ is the viscosity of a liquid, $\mathbf{u}$ is the velocity, ρ is the density, P is the pressure, T is the temperature, k is the thermal conductivity, C_p is the heat capacity, D is the diffusion coefficient, and R is the source density. The parameter values used were taken from the related literature, and finite element simulation was carried out to solve the equations.[38]

Conflict of Interest: The authors declare no competing financial interest.

Acknowledgment. This research was supported by Basic Science Research Program through the National Research Foundation of Korea (NRF) funded by the Ministry of Education, Science and Technology (NRF-2013R1A1A2059827). This work was also supported by Korea Ministry of Environment as "Converging Technology Project" (grant code: 2012000670001).

Supporting Information Available: Stamp design and fabrication procedure, details on the fabrication of a film heater array system, description of a membrane electrode assembly, and explanation of simulation and measurements. This material is available free of charge *via* the Internet at http://pubs.acs.org.

REFERENCES AND NOTES

1. Priolo, F.; Gregorkiewicz, T.; Galli, M.; Krauss, T. F. Silicon Nanostructures for Photonics and Photovoltaics. *Nat. Nanotechnol.* **2014**, *9*, 19–32.
2. Qin, D.; Xia, Y.; Whitesides, G. M. Soft Lithography for Micro- and Nanoscale Patterning. *Nat. Protoc.* **2010**, *5*, 491–502.
3. Guo, L. J. Nanoimprint Lithography: Methods and Material Requirements. *Adv. Mater.* **2007**, *19*, 495–513.
4. Zhang, K.; Fu, Q.; Pan, N.; Yu, X.; Liu, J.; Luo, Y.; Wang, X.; Yang, J.; Hou, J. Direct Writing of Electronic Devices on Graphene Oxide by Catalytic Scanning Probe Lithography. *Nat. Commun.* **2012**, *3*, 1194.
5. Satyaprasad, A.; Jain, V.; Nema, S. K. Deposition of Superhydrophobic Nanostructured Teflon-like Coating Using Expanding Plasma Arc. *Appl. Surf. Sci.* **2007**, *253*, 5462–5466.
6. Alegria, L. D.; Schroer, M. D.; Chatterjee, A.; Poirier, G. R.; Pretko, M.; Patel, S. K.; Petta, J. R. Structural and Electrical Characterization of Bi_2Se_3 Nanostructures Grown by Metal-Organic Chemical Vapor Deposition. *Nano Lett.* **2012**, *12*, 4711–4714.

7. Liao, X.; Brown, K. A.; Schmucker, A. L.; Liu, G.; He, S.; Shim, W.; Mirkin, C. A. Desktop Nanofabrication with Massively Multiplexed Beam Pen Lithography. *Nat. Commun.* **2013**, *4*, 2103.
8. Li, B.; Tahara, K.; Adisoejoso, J.; Vanderlinden, W.; Mali, K. S.; De Gendt, S.; Tobe, Y.; De Feyter, S. Self-Assembled Air-Stable Supramolecular Porous Networks on Graphene. *ACS Nano* **2013**, *7*, 10764–10772.
9. Harada, A.; Kobayashi, R.; Takashima, Y.; Hashidzume, A.; Yamaguchi, H. Macroscopic Self-Assembly through Molecular Recognition. *Nat. Chem.* **2011**, *3*, 34–37.
10. Ahn, S. H.; Guo, L. J. Large-Area Roll-to-Roll and Roll-to-Plate Nanoimprint Lithography: A Step toward High-Throughput Application of Continuous Nanoimprinting. *ACS Nano* **2009**, *3*, 2304–2310.
11. Austin, M. D.; Chou, S. Y. Fabrication of 70 nm Channel Length Polymer Organic Thin-Film Transistors Using Nanoimprint Lithography. *Appl. Phys. Lett.* **2002**, *81*, 4431.
12. Jeon, S.; Jang, J. Y.; Youn, J. R.; Jeong, J. H.; Brenner, H.; Song, Y. S. Fullerene Embedded Shape Memory Nanolens Array. *Sci. Rep.* **2013**, *3*, 3269.
13. Jung, G. Y.; Johnston-Halperin, E.; Wu, W.; Yu, Z.; Wang, S. Y.; Tong, W. M.; Li, Z.; Green, J. E.; Sheriff, B. A.; Boukai, A.; *et al.* Circuit Fabrication at 17 nm Half-Pitch by Nanoimprint Lithography. *Nano Lett.* **2006**, *6*, 351–354.
14. Campoccia, D.; Montanaro, L.; Arciola, C. R. A Review of the Biomaterials Technologies for Infection-Resistant Surfaces. *Biomaterials* **2013**, *34*, 8533–8554.
15. Carson, L.; Chau, P. K. W.; Earle, M. J.; Gilea, M. A.; Gilmore, B. F.; Gorman, S. P.; McCann, M. T.; Seddon, K. R. Antibiofim Activities of 1-Alkyl-3-methylimidazolium Chloride Ionic Liquids. *Green Chem.* **2009**, *11*, 492–497.
16. Dheilly, A.; Soum-Soutera, E.; Klein, G. L.; Bazire, A.; Compere, C.; Haras, D.; Dufour, A. Antibiofilm Activity of the Marine Bacterium *Pseudoalteromonas* sp. Strain 3J6. *Appl. Environ. Microbiol.* **2010**, *76*, 3452–3461.
17. Pooringa, A. T.; Smit, J.; van der Mei, H. C.; Busscher, H. J. Electric Field Induced Desorption of Bacteria from a Conditioning Film Covered Subtratum. *Biotechnol. Bioeng.* **2001**, *76*, 395–399.
18. Hong, S. H.; Jeong, J.; Shim, S.; Kang, H.; Kwon, S.; Ahn, K. H.; Yoon, J. Effect of Electric Currents on Bacterial Detachment and Inactivation. *Biotechnol. Bioeng.* **2008**, 100.
19. Xu, H.; Liu, Y. Control and Cleaning of Membrane Biofouling by Energy Upcoupling and Cellular Communication. *Environ. Sci. Technol.* **2011**, *45*, 595–601.
20. Lawrence, J. R.; Neu, T. R.; Swerhone, G. D. W. Application of Multiple Parameter Imaging for the Quantification of Algal, Bacterial and Exopolymer Components of Microbial Biofilms. *J. Microbiol. Methods* **1998**, *32*, 253–261.
21. Upadhyaya, L.; Singh, J.; Agarwal, V.; Tewari, R. P. Recent Progress in Antimicrobial Applications of Nanostructured Materials. *J. Nanopharmaceutics Drug Delivery* **2013**, *1*, 4–17.
22. Salta, M.; Wharton, J. A.; Stoodley, P.; Dennington, S. P.; Goodes, L. R.; Werwinski, S.; Mart, U.; Wood, R. J.; Stokes, K. R. Designing Biomimetic Antifouling Surfaces. *Philos. Trans. R. Soc., A* **2010**, *368*, 4729–4754.
23. Desrousseaux, C.; Sautou, V.; Descamps, S.; Traore, O. Modification of the Surfaces of Medical Devices To Prevent Microbial Adhesion and Biofilm Formation. *J. Hosp. Infect.* **2013**, *85*, 87–93.
24. Crawford, R. J.; Webb, H. K.; Truong, V. K.; Hasan, J.; Ivanova, E. P. Surface Topographical Factors Influencing Bacterial Attachment. *Adv. Colloid Interface Sci.* **2012**, *179–182*, 142–149.
25. Mitik-Dineva, N.; Wang, J.; Truong, V. K.; Stoddart, P.; Malherbe, F.; Crawford, R. J.; Ivanova, E. P. *Escherichia coli*, *Pseudomonas aeruginosa*, and *Staphylococcus aureus* Attachment Patterns on Glass Surfaces with Nanoscale Roughness. *Curr. Microbiol.* **2009**, *58*, 268–273.
26. Bryers, J. D. Medical Biofilms. *Biotechnol. Bioeng.* **2008**, *100*, 1–18.
27. Chen, W. F.; Muckerman, J. T.; Fujita, E. Recent Developments in Transition Metal Carbides and Nitrides as Hydrogen Evolution Electrocatalysts. *Chem. Commun.* **2013**, *49*, 8896–8909.
28. Lan, E. I.; Ro, S. Y.; Liao, J. C. Oxygen-Tolerant Coenzyme A-Acylating Aldehyde Dehydrogenase Facilitates Efficient Photosynthetic *n*-Butanol Biosynthesis in Cyanobacteria. *Energy Environ. Sci.* **2013**, *6*, 2672–2681.
29. Strik, D. P.; Terlouw, H.; Hamelers, H. V.; Buisman, C. J. Renewable Sustainable Biocatalyzed Electricity Production in a Photosynthetic Algal Microbial Fuel Cell (PAMFC). *Appl. Microbiol. Biotechnol.* **2008**, *81*, 659–668.
30. Chiao, M.; Lam, K. B.; Lin, L. Micromachined Microbial and Photosynthetic Fuel Cells. *J. Micromech. Microeng.* **2006**, *16*, 2547–2553.
31. Rosenbaum, M.; He, Z.; Angenent, L. T. Light Energy to Bioelectricity: Photosynthetic Microbial Fuel Cells. *Curr. Opin. Biotechnol.* **2010**, *21*, 259–264.
32. Rosenbaum, M.; Schroder, U. Photomicrobial Solar and Fuel Cells. *Electroanalysis* **2010**, *22*, 844–855.
33. Strik, D. P.; Timmers, R. A.; Helder, M.; Steinbusch, K. J.; Hamelers, H. V.; Buisman, C. J. Microbial Solar Cells: Applying Photosynthetic and Electrochemically Active Organisms. *Trends Biotechnol.* **2011**, *29*, 41–49.
34. Yagishita, T.; Sawayama, S.; Tsukahara, K.; Ogi, T. Effects of Intensity of Incident Light and Concentrations of *Synechococcus* sp, and 2-Hydroxy-1,4-naphthoquinone on the Current Output of Photosynthetic Electrochemical Cell. *Sol. Energy* **1997**, *61*, 347–353.
35. Zou, Y.; Pisciotta, J.; Billmyre, R. B.; Baskakov, I. V. Photosynthetic Microbial Fuel Cells with Positive Light Response. *Biotechnol. Bioeng.* **2009**, *104*, 939–946.
36. Denkhaus, E.; Meisen, S.; Telgheder, U.; Wingender, J. Chemical and Physical Methods for Characterisation of Biofilms. *Microchim. Acta* **2007**, *158*, 1–27.
37. Uan-Zo-Li, J. T. The Effects of Structure, Humidity and Aging on the Mechanical Properties of Polymeric Ionomers for Fuel Cell Applications, Ph.D. Thesis, Virginia Polytechnic Institute, 2001.
38. Song, Y. S.; Lin, R. L.; Montesano, G.; Durmus, N. G.; Lee, G.; Yoo, S. S.; Kayaalp, E.; Haeggstrom, E.; Khademhosseini, A.; Demirci, U. Engineered 3D Tissue Models for Cell-Laden Microfluidic Channels. *Anal. Bioanal. Chem.* **2009**, *395*, 185–193.